Applied Catalysis B: Environmental 305 (2022) 121047

Contents lists available at ScienceDirect

Applied Catalysis B: Environmental

journal homepage: www.elsevier.com/locate/apcatb

Converting water impurity in organic solvent into hydrogen and hydrogen peroxide by organic semiconductor photocatalyst

Zhenyu Wu [a], Xiting Wang [a], Yi Li [a], Han Zhao [a], Jiawei Wang [a], Hui Huang [a,*], Yang Liu [a,*], Zhenhui Kang [a,b,**]

[a] Institute of Functional Nano & Soft Materials (FUNSOM), Jiangsu Key Laboratory for Carbon-Based Functional Materials & Devices, Soochow University, 199 Ren'ai Road, Suzhou 215123, Jiangsu, China

[b] Macao Institute of Materials Science and Engineering, Macau University of Science and Technology, Taipa 999078, Macau SAR, China

ARTICLE INFO

Keywords:
Organic photocatalyst
Hydrogen
Hydrogen peroxide
Transient photovoltage
Water removal

ABSTRACT

Photocatalytic water-splitting to generate hydrogen (H_2) and hydrogen peroxide (H_2O_2) is a green and renewable method to convert solar energy into chemical energy. The water impurity in organic solvents is usually hard to be removed. Here, we firstly used an organic semiconductor (DAnTMS) synthesized from 9,10-dibromoanthracene and trimethylsilylacetylene to convert the water impurity in organic solvent into H_2 and H_2O_2 by photocatalysis. Under visible light, for 300.0 μL water in 20.0 mL methyl cyanide (MeCN) system, the DAnTMS catalyst can produce H_2 and H_2O_2 with rate of 245.9 μmol g^{-1} h^{-1} and 3923.4 μmol g^{-1} h^{-1}, respectively. Furthermore, a practical photocatalytic experiment was performed in 20.0 mL commercially available MeCN (99.8%, $H_2O \leq$ 0.01%) with 10.0 mg DAnTMS as catalyst, in which, the total 15.4 μmol H_2 and 176.7 μmol H_2O_2 were generated after 12 h reaction, suggesting the water impurity in MeCN was completely removed. In present catalytic system, on DAnTMS, O_2 and H_2O are reduced into H_2O_2 and H_2, respectively, while, H_2O is oxidized into H_2O_2 through a $2e^-$ pathway.

1. Introduction

As one of the most promising ways to solve the problem of global energy crisis and environment pollution, visible light driven photocatalytic water-splitting has been paid much attention to in current photocatalysis studies [1–5]. Hydrogen (H_2) and hydrogen peroxide (H_2O_2) are two main products of photocatalytic water-splitting. H_2 has the potential to substitute for fossil fuels due to its environmental friendliness and renewability, while H_2O_2 is an important chemical material for many industries [6–11]. The organic semiconductor used as water-splitting catalyst was first attempted by Yanagida et al. in 1985, who used linear polymer as the photocatalyst for H_2 evolution under the irradiation of UV-light ($\lambda > 366$ nm) [12]. Since then, organic semiconductors have raised global attention. Organic semiconductors own unique advantages compared with inorganic semiconductors, such as low cost, broad light absorbance in visible region, flexibly and precisely tuned molecular and photoelectrical properties and so on [4,13–17]. On the other hand, there is always water impurity in industrial chemical organic reagents, which is hard to remove [18,19]. The traditional method of distillation is extremely energy-intensive and thus high-cost [20–22]. Therefore, it is meaningful to find a low-cost and energy-saving way to remove the water impurity. Utilization of organic photocatalyst to convert this kind of water into value-added chemicals seems a novel and promising way. Note that, this proposed catalytic system should meet the multiple requirements for photocatalysts, from the visible light excitation to the inability of any cocatalyst and sacrificial agents [23].

Here, a reported organic semiconductor (DAnTMS) synthesized from 9,10-dibromoanthracene (DAn) and trimethylsilylacetylene (TMS) was prepared and firstly used in water removal in methyl cyanide (MeCN, 99.8%, $H_2O \leq 0.01\%$). Then, the photocatalytic properties of DAnTMS in MeCN with addition of trace amount of water was investigated, which achieved the efficient photocatalytic production of H_2 and H_2O_2 without using any cocatalyst and sacrificial agent. Under visible light, when

* Corresponding authors.
** Corresponding author at: Institute of Functional Nano & Soft Materials (FUNSOM), Jiangsu Key Laboratory for Carbon-Based Functional Materials & Devices, Soochow University, 199 Ren'ai Road, Suzhou 215123, Jiangsu, China.
E-mail addresses: hhuang0618@suda.edu.cn (H. Huang), yangl@suda.edu.cn (Y. Liu), zhkang@suda.edu.cn (Z. Kang).

https://doi.org/10.1016/j.apcatb.2021.121047
Received 14 November 2021; Received in revised form 23 December 2021; Accepted 26 December 2021
Available online 29 December 2021

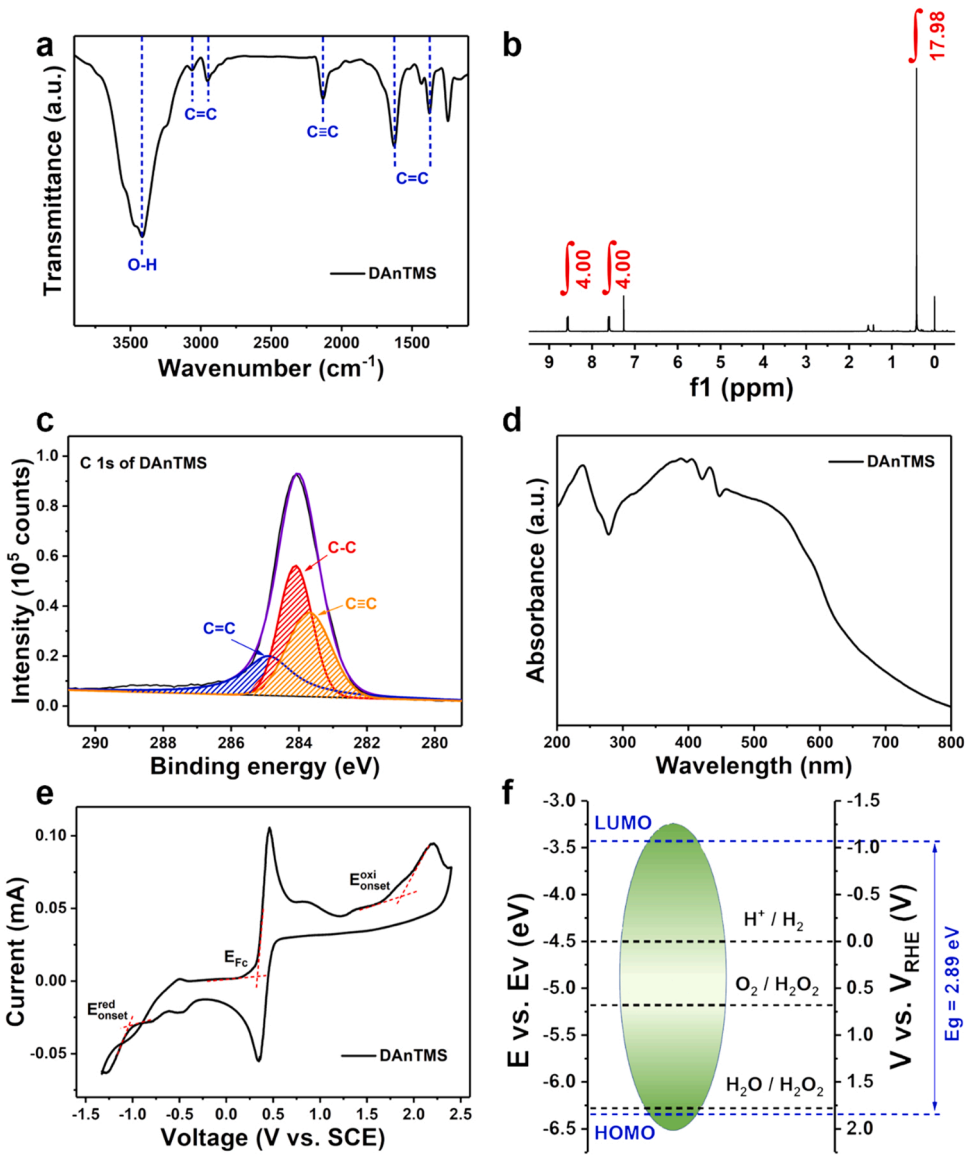

Fig. 1. Characterization and energy structure of the as-prepared DAnTMS. (a) The FT-IR spectrum. (b) ^{1}H NMR spectrum. (c) The high resolution XPS spectrum of C 1s (d) The UV–vis spectrum of DAnTMS powders. (e) The CV curve. (f) The diagram of energy band structure.

300.0 μL pure water added, the catalyst could produce H_2 with a maximum rate of 245.9 μmol g^{-1} h^{-1} and H_2O_2 with a maximum rate of 3923.4 μmol g^{-1} h^{-1} in 20.0 mL MeCN. Furthermore, a practical photocatalytic experiment was also performed in 20.0 mL commercially available MeCN (99.8%, $H_2O \leq 0.01\%$) with 10.0 mg DAnTMS as catalyst, where 15.4 μmol H_2 and 176.7 μmol H_2O_2 were generated, which completely removed the water impurity. On DAnTMS, O_2 was reduced into H_2O_2 and H_2O was reduced into H_2 both through the $2e^-$ pathway. Also, H_2O was oxidated into H_2O_2 through a $2e^-$ pathway. This work demonstrated the homogeneous water photo-splitting to produce clean chemical energy by organic molecular catalysts.

2. Experimental

2.1. Materials

TMS (GC, 98%) and DAn (GC, 98%) were purchased from TCI. THF (GC, 99.5%), diisopropyamine (GC, 99.0%), $Pd(PPh_3)_2Cl_2$ and MeCN (98%, $H_2O \leq 0.01\%$)were purchased from Macklin. CuI (99.5%) was purchased from Sigma-Aldrich.

2.2. Synthesis of DAnTMS organic photocatalyst

DAnTMS was synthesized through the cross-coupling reaction. After the final product was extracted and dried, the dark-red powder was obtained. The detailed synthetic method of DAnTMS is shown in the Supporting Information.

2.3. Photocatalytic experiments of DAnTMS

In brief, certain mass of DAnTMS and 20 mL MeCN were mixed and ultrasonic treated to form a uniform and transparent solution. Then, certain volume of ultra-pure water (0.1, 0.2, 0.3, 0.4 and 0.5 mL) was added into the solution. After that, all the reactants were transferred to a 40 mL glass bottle. After sealing treatment, the bottle was irradiated under visible light (420 nm $\leq \lambda \leq$ 700 nm, light intensity = 86.11 mW/cm^2) for a period of time under constant stirring.

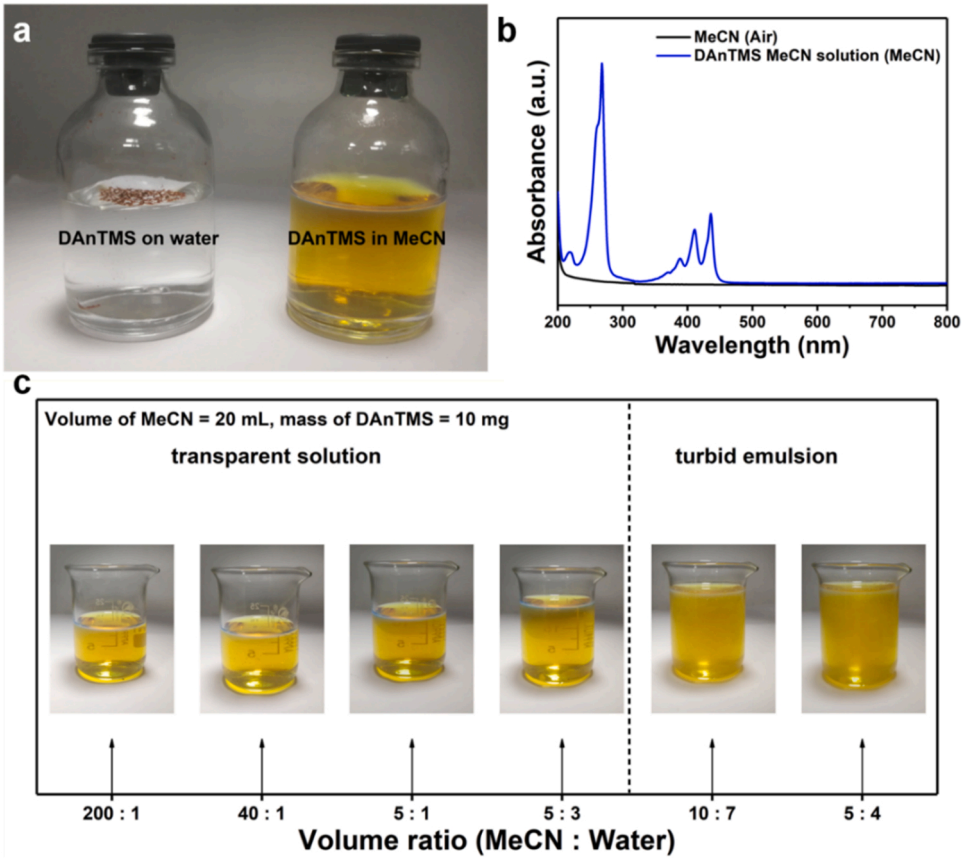

Fig. 2. (a) The image of 10 mg DAnTMS floating on 20 mL water and dissolving in 20 mL MeCN. (b) The UV–vis spectra of MeCN (reference: air) and DAnTMS MeCN solution (reference: MeCN). (c) The change of DAnTMS MeCN solution with different volume ratio between MeCN and water (Volume of MeCN = 20 mL and mass of DAnTMS = 10 mg).

3. Results and discussion

3.1. Characterization of the organic photocatalyst

The DAnTMS organic semiconductor was synthesized through the reported work and its molecular formula is shown in Fig. S1. The raw materials were heated and refluxed, and then extracted and dried to finally obtain a dark red solid powder (98% yield). In order to make sure that DAnTMS was successfully synthesized again, Fourier transform infrared spectroscopy (FT-IR) was carried out to investigate the surface functional groups of DAnTMS, displayed in Fig. 1**a**. The peaks located at about 3060, 2950, 1627 and 1380 cm^{-1} can be ascribed to the stretch vibration of C=C and the peak caused by the stretch vibration of C≡C is located at 2129 cm^{-1} [24,25]. What's more, ^{1}H nuclear magnetic resonance (NMR) measurements were carried out to identify the structure of the synthesized compound, shown in Fig. 1**b**. The peaks at 0.424 ppm can be ascribed to the characteristics of the methyl groups of trimethylsilyl. The four peaks in the range from 7.593 to 7.618 ppm and the four peaks in the range from 8.558 to 8.583 ppm can be attributed to the aromatic protons (detailed figure of ^{1}H NMR spectra in the two ranges are shown in Fig. S2.) [26]. Furthermore, the integral area of the three groups of peaks were calculated to be 17.98, 4.00 and 4.00, exactly corresponding to all the protons on the synthesized DAnTMS in three different chemical environments, which confirms the successful synthesis of the DAnTMS compound. Furthermore, the full X-ray photoelectron spectroscopy (XPS) were used to investigate the elemental composition and the chemical bonds of the photocatalyst. As is shown in Fig. S3a, the full XPS spectrum suggests that DAnTMS is only composed of C and Si elementals. The high resolution XPS spectrum of C 1s is presented in Fig. 1**c**, which can be deconvoluted into three peaks at 284.2, 284.8 and 283.7 eV, ascribed to C-C, C=C, and C≡C bonds, respectively [27,28]. In addition, the high resolution XPS spectrum of Si 2p is shown in Fig. S3b, which is only composed of one peak at 100.3 eV, which can be attributed to the Si-C bond [29,30]. The morphology of the as-prepared DAnTMS is shown in Fig. S4, explored by scanning electron microscopy (SEM) and transmission electron microscopy (TEM). From the image of SEM, DAnTMS exhibits a needle-like structure, whose length is around 4–6 μm. The TEM image further confirms the results, shown in the inset image of Fig. S4.

The ultraviolet-visible (UV–vis) spectrum of DAnTMS powder is presented in Fig. 1**d**, where DAnTMS powder exhibits strong absorption in the region of ultraviolet and further extends to about 630 nm, suggesting that DAnTMS has a good ability to absorb light in the range of UV–vis light, thus proving the feasibility of photocatalysis from the aspect of light absorption. Cyclic voltammetry (CV) was used to investigate the energy band structure of DAnTMS and the results are displayed in Fig. 1**e** [1,8,31]. From the CV curve, the highest occupied molecular orbital (HOMO) and the lowest unoccupied molecular orbital (LUMO) can be calculated through the formula (1) and (2) provided in Supporting Information. The HOMO and LUMO were determined to be − 6.33 eV and − 3.44 eV, respectively and the energy gap of DAnTMS was calculated to be 2.89 eV. Therefore, a diagram of the energy band structure of DAnTMS was further shown in Fig. 1**f**, in which the LUMO of DAnTMS is more negative than the potential of H^{+} reduction to H_2 and O_2 reduction to H_2O_2 and the HOMO of it is more positive than the potential of H_2O oxidation to H_2O_2. Therefore, it is reasonable that DAnTMS is able to catalyze H_2O into H_2 and H_2O_2 under the irradiation of visible light from the perspective of thermodynamics [32]. Therefore, taking all the results of characterization and energy band structure, the reported product of DAnTMS was successfully synthesized.

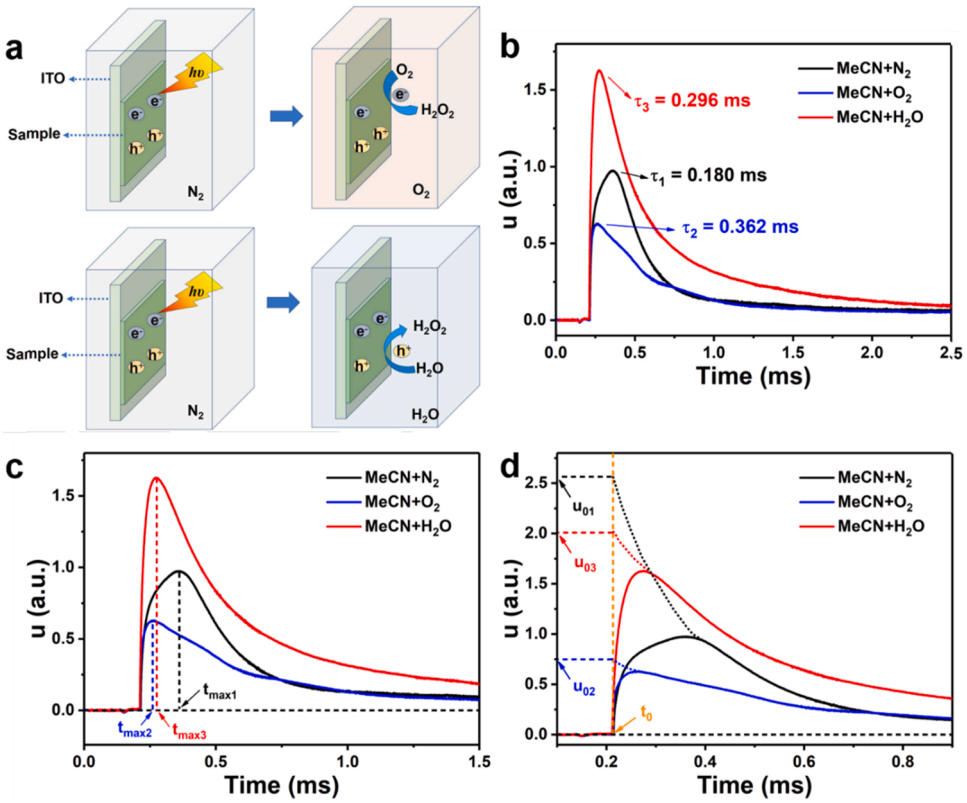

Fig. 3. Comparison of the in-situ TPV curves of DAnTMS under different atmospheres. (a) The schematic diagram of TPV measurements. (b) Relaxation in-situ TPV curves of DAnTMS under N_2 saturated MeCN, O_2 saturated MeCN and 0.5 vol% H_2O/MeCN (v/v) and the corresponding attenuation constants (τ) of charge recombination process. (c) Charge extraction rate (t_{max}) under different atmospheres. (d) The extrapolation of TPV curves.

As shown in Fig. 2**a**, the 10 mg DAnTMS is floating on 20 mL water and well dissolving in 20 mL MeCN, indicating that DAnTMS is hydrophobic and not suitable for the catalysis in pure water. The results of contact angel (CA) test of DAnTMS are shown in Fig. S5, where the left and right CA of DAnTMS are 126.7° and 126.6°, respectively, further suggesting the hydrophobicity of DAnTMS. Therefore, the homogeneous catalytic system formed after DAnTMS dissolving in MeCN is beneficial for photocatalysis. Furthermore, the ability of light absorbance of MeCN and DAnTMS MeCN solution is investigated by UV–vis spectrophotometer, the results of which are displayed in Fig. 2**b**. Pure MeCN only exhibits strong absorbance in far UV region (reference: air), suggesting that the ability of absorbing light comes from DAnTMS itself. DAnTMS MeCN solution shows several absorbance peaks in UV–vis region (reference: MeCN). The peaks located at 217 and 268 nm correspond to the π – π * and n – π * transition on the benzene ring, respectively [33]. Three peaks of 389, 411 and 436 nm can be ascribed to the absorbance peaks of anthracene structure [34]. The UV–vis spectra of DAn and TMS can further help to interpret the UV–vis spectrum of DAnTMS. As shown in Fig. S6, for DAn, the three peaks located at 364, 384 and 406 nm can be attributed to the absorbance peaks of anthracene structure. The peaks at 228 and 286 nm can be attributed to the π – π * and n – π * transition, respectively. For TMS, the two peaks at 213 and 285 nm can be attributed to the π – π * and n – π * transition, respectively. The effects of additional water volume on the ability of light absorbance were further studied, shown in Fig. S7. The changes of absorbances corresponding to the five peaks (217, 268, 389, 411 and 436 nm) of UV–vis spectrum are small, proving that effect of additional water on the light absorbance of the system is negligible. Finally, the change of DAnTMS MeCN solution with different volume ratio between MeCN and water was explored, displayed in Fig. 2**c**. For 20 mL MeCN with 10 mg DAnTMS, only when the volume ratio between MeCN and water reaches 10:7, the heterogeneous turbid emulsion replaces the original homogeneous transparent solution. This further proves that it is feasible to use the homogeneous catalytic system for the photocatalysis of MeCN solution with trace water content.

The TPV measurements were further performed to explore the photocatalytic properties and charge transfer process over DAnTMS before the photocatalytic experiments [35–37]. The principle of TPV measurements is schematically demonstrated in Fig. 3**a**. DAnTMS was filmed onto an ITO electrode, then different MeCN solution (N_2 saturated, O_2 saturated and 0.5 vol% H_2O) were sprayed onto the DAnTMS film to form a thin liquid layer. A pulse laser of 355 nm (5 ns) was used to excite DAnTMS and the TPV signals were collected by a computer simultaneously. Under N_2 saturated MeCN, after being excited, the electrons of DAnTMS will transfer to the ITO electrode and the charge recombination process also can be identified. Furthermore, under O_2 saturated MeCN or 0.5 vol% H_2O/MeCN (v/v), O_2 or H_2O will consume electrons or holes, leading to the change of charges collected by ITO. The more electrons collected by ITO electrode, the stronger the photovoltage intensity will be and vice versa. Therefore, certain chemical reactions also can be identified by the change of TPV signals. According to the formula, U = Q / C, transient photovoltage intensity (u) can represent the relative amount of charge (Q).

Fig. 3**b** exhibits the TPV relaxation curves of DAnTMS under N_2, O_2 saturated MeCN and 0.5 vol% H_2O/MeCN (v/v), respectively. The photovoltage intensity of DAnTMS under O_2 saturated MeCN is lower than that under N_2 saturated MeCN. This can be ascribed to O_2 reduction that consumes electrons. When the test was performed under 0.5 vol% H_2O/MeCN (v/v), the photovoltage intensity becomes higher than that under N_2 saturated MeCN, suggesting that H_2O oxidation reaction may occur, which consumes holes. Also, the attenuation constants (τ) were used to estimate the charge recombination rates of DAnTMS under different atmospheres [38–40]. It is notable that τ under N_2 saturated MeCN ($\tau_1 = 0.180$ ms) is obviously smaller than that under O_2 saturated

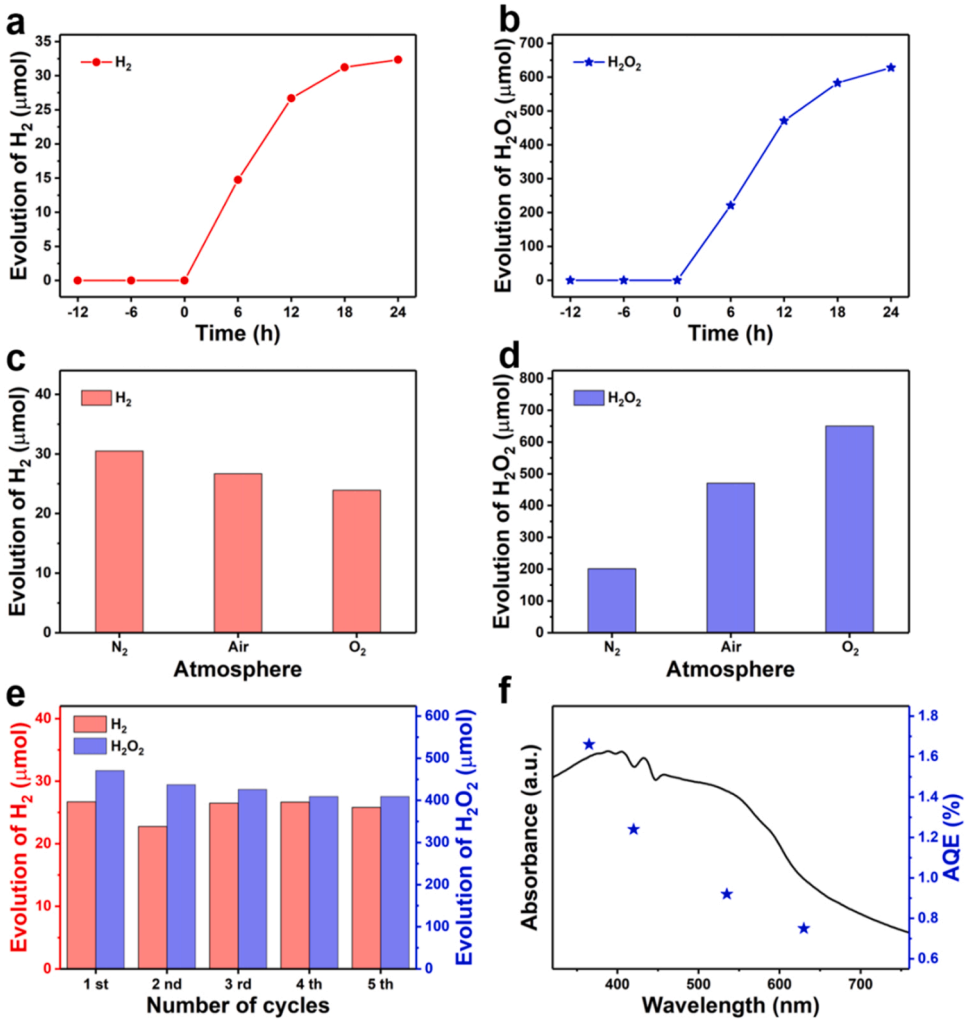

Fig. 4. Photocatalytic performances of 10.0 mg DAnTMS in 20.0 mL MeCN with additional 300.0 μL pure water. (a, b) Production of H_2 and H_2O_2 versus time. (c, d) Production of H_2 and H_2O_2 in N_2, air and O_2 after 12 h irradiation. (e) Stability tests of DAnTMS. (f) The UV–vis absorbance spectrum and the corresponding AQE under different wavelengths of incident light (365, 420, 535 and 630 nm).

MeCN ($\tau_2 = 0.362$ ms) and 0.5 vol% H_2O/MeCN (v/v) ($\tau_3 = 0.296$ ms), indicating that, without any reaction, the charges on the surface of DAnTMS recombine through a rapid process.

Fig. 3**c** displays the charge extraction rate (t_{max}) of DAnTMS under different atmospheres, where the t_{max1} ($t_{max1} = 0.147$ ms) is sharply slower than those of t_{max2} ($t_{max2} = 0.045$ ms) and t_{max3} ($t_{max3} = 0.059$ ms). These results suggest that the surface of DAnTMS is unfavorable for the charge transfer between the catalyst and the electrode under N_2 saturated MeCN. The great differences of τ and t_{max} indicate together that, under N_2 saturated MeCN, it is hard for electrons of DAnTMS excited by laser to reach the ITO electrode while the excited electrons recombine rapidly. Different from chemical reaction rate control steps under O_2 saturated MeCN and 0.5 vol% H_2O/MeCN (v/v), the charge transfer rate control step under N_2 saturated MeCN leads to an inaccurate photovoltage intensity detected by the ITO electrode. Therefore, as shown in Fig. 3**d**, extrapolation is applied on the TPV curves. Three TPV curves are extrapolated to the initial time point t_0 and the corresponding photovoltage u_0 was calculated, which represents the maximum surficial amount of charge extracted from the catalyst. For the atmosphere of N_2 saturated MeCN ($u_{01} = 2.574$) and 0.5 vol% H_2O/MeCN (v/v) ($u_{03} = 2.030$), $\Delta Q(N_2/H_2O) = u_{01} - u_{03} = 0.544$, indicating that compared with atmosphere of N_2 saturated MeCN, the introduction of H_2O actually decreases the maximum surficial amount of charge. This suggests that apart from H_2O oxidation reaction, H_2O reduction reaction occurs and the rate of H_2O reduction is faster than that of H_2O oxidation. Similarly, for the atmosphere of N_2 saturated MeCN and O_2 saturated MeCN ($u_{03} = 0.756$), $\Delta Q(N_2/O_2) = u_{01} - u_{02} = 1.818$, thus suggesting that the rate of O_2 reduction reaction is also rapid and is more rapid than that of H_2O reduction.

3.2. Photocatalytic performances of the photocatalyst

Photocatalytic experiments were further carried out to study the photocatalytic activity of DAnTMS. Photocatalytic activity of 10.0 mg DAnTMS in 20.0 mL MeCN with additional 300.0 μL pure water was first investigated. The production of H_2 and H_2O_2 with the change of irradiation time are shown in Fig. 4**a & b**, respectively. For both the production of H_2 and H_2O_2, in the first 6 and 12 h, the rates were obviously faster than that of 18 and 24 h. The largest rate of H_2 production occurs in 6 h, which is 245.9 μmol g^{-1} h^{-1} and the largest rate of H_2O_2 production occurs in 12 h, which is 3923.4 μmol g^{-1} h^{-1}. The decrease of rates is caused by H_2O_2 poisoning of the photocatalyst, which can be confirmed by the test of H_2O_2 poisoning. As shown in Fig. S8, the *i*-t curve is used to prove the H_2O_2 poisoning effect on DAnTMS. When 5 mL 30% H_2O_2 was added into 0.1 M Na_2SO_4 solution, a sharp decrease of the current is observed, thus indicating that H_2O_2 can poison the photocatalyst. The mechanism of H_2 and H_2O_2 production of DAnTMS were also investigated preliminarily by the atmosphere tests. As

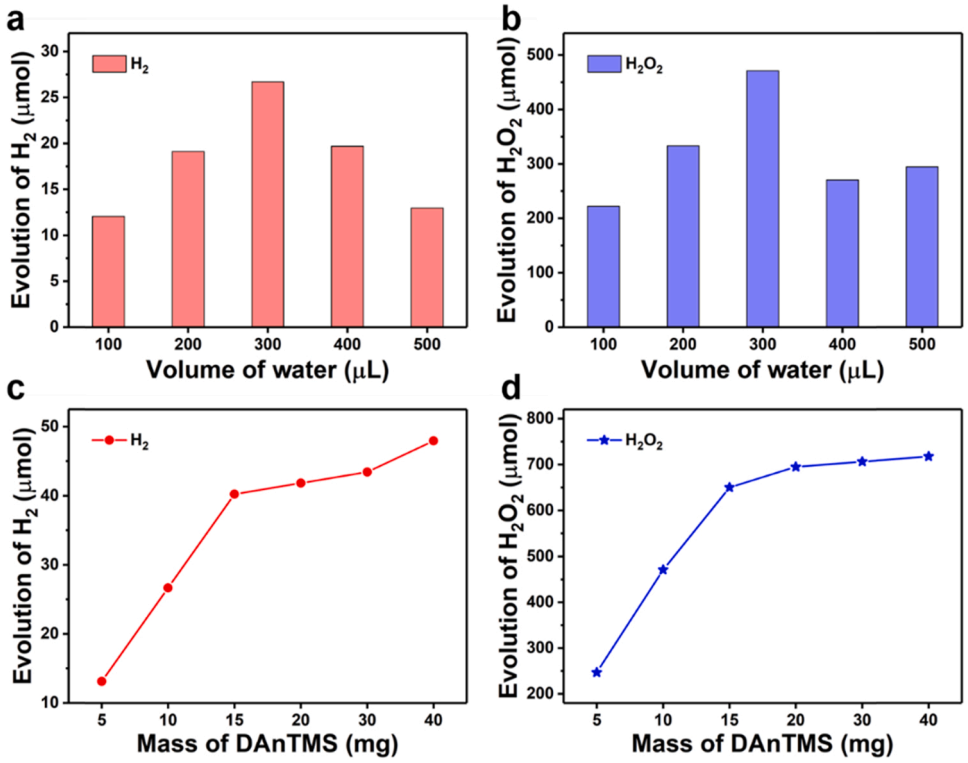

Fig. 5. Exploration of the effects of water content and catalyst concentration on photocatalytic performances of DAnTMS. (a, b) Production of H_2 and H_2O_2 of 10.0 mg DAnTMS in 20.0 mL MeCN with change of additional volume of water. (c, d) Production of H_2 and H_2O_2 with change of mass of DAnTMS in 20.0 mL MeCN with additional 300.0 μL pure water.

depicted in Fig. 4**c** & **d**, after 12 h irradiation, the production of H_2 increases under N_2 atmosphere and decreases under O_2 atmosphere while the production of H_2O_2 exhibits the opposite trend, which decreases under N_2 atmosphere and increases under O_2 atmosphere. These results suggest that the production of H_2O_2 is related to O_2 reduction and there exists a competitive relationship between H_2O reduction and O_2 reduction. Fig. 4**e** displays the results of stability tests of DAnTMS. In the first cycling experiments, total four bottle of reactants (10.0 mg

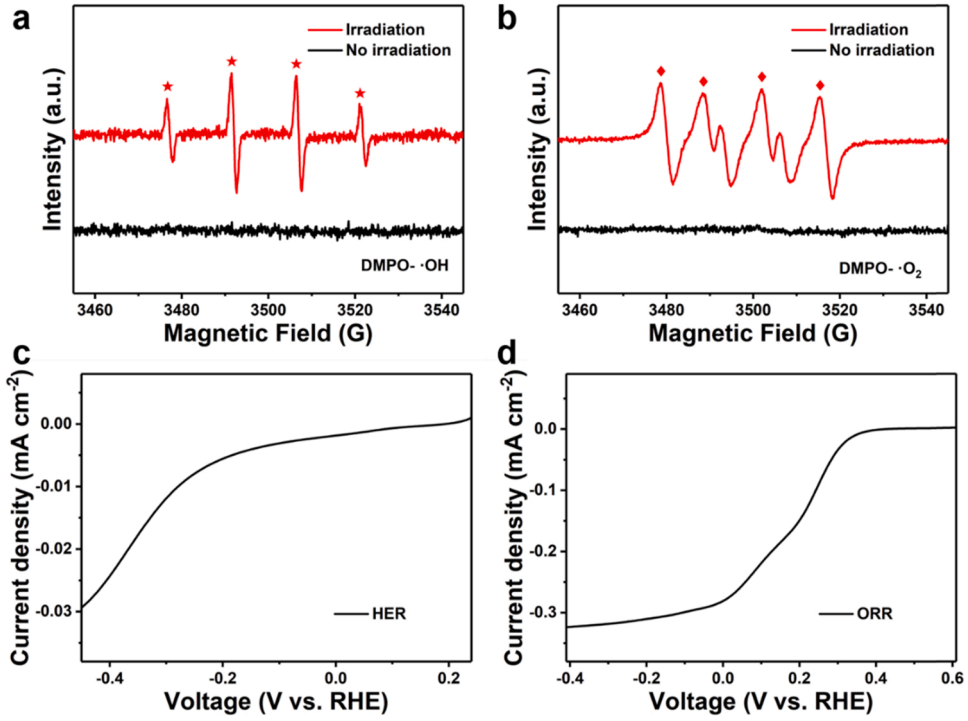

Fig. 6. Exploration of the mechanism of DAnTMS-mediated photocatalytic process. DMPO spin-trapping EPR spectra of DAnTMS of (a) superoxide radical and (b) hydroxyl radical. LSV curves of DAnTMS of (c) HER and (d) ORR.

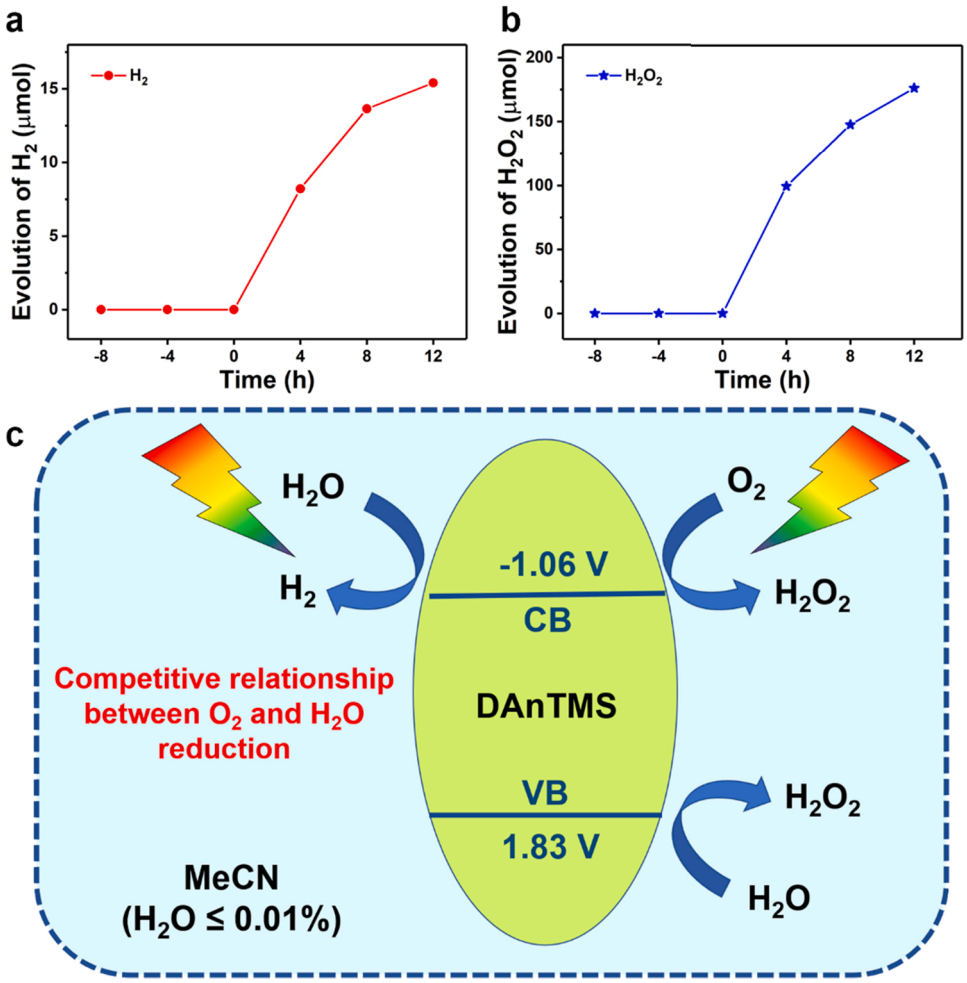

Fig. 7. Photocatalytic performances of DAnTMS in commercially available MeCN ($H_2O \leq 0.01\%$). (a, b) Production of H_2 and H_2O_2 versus time. (c) The schematic diagram of DAnTMS mediated photocatalysis of water splitting.

DAnTMS, 20.0 mL MeCN and 300.0 μL water in each bottle) were irradiated for 12 h. After that, 2.0 mL gas was drawn from each bottle and injected into the gas chromatograph for further analysis. 1.0 mL solution was extracted from each bottle for further titration. After calculating the yield of H_2 and H_2O_2, all the remaining solution was transferred into a 100.0 mL beaker and dry under 60 ℃ to remove all the organic solvents, water and hydrogen peroxide, thus obtaining DAnTMS powder. The mass of remaining DAnTMS was enough for another 3 comparison experiments for the second cycling experiments. Similarly, these steps were applied to the third, fourth and fifth cycling experiments. The catalyst exhibits excellent stability for five circles, each of which is performed for 12 h. Lastly, experiments for calculating the apparent quantum efficiency (AQE) of the photocatalyst under lights of different wavelengths were carried out. As displayed in Fig. 4**f**, the results are in accordance with the capability of light absorption of DAnTMS obtained by the UV-Vis spectrum, where the AQE of DAnTMS reaches its highest value of 1.66 % under the light of 365 nm and exhibits its lowest value of 0.75 % under the light of 630 nm.

The effects of water content and catalyst concentration on photocatalytic performances of DAnTMS were also studied by another series of photocatalytic experiments. The results of photocatalytic activity of 10.0 mg DAnTMS irradiated for 12 h in 20.0 mL MeCN with different additional volumes of pure water (100.0, 200.0, 300.0, 400.0 and 500.0 μL) are shown in Fig. 5**a & b**. The photocatalytic performances of DAnTMS are the best when the additional volume of water is 300.0 μL, with 26.7 μmol H_2 and 470.8 μmol H_2O_2 evolution. Here, atmosphere tests for the volume of additional water of 100.0, 200.0, 400.0 and 500.0 μL were also performed and the results are shown in Fig. S9. After 12 h irradiation, the production of H_2 decreases and production of H_2O_2 increases with the increasement of O_2 concentration, further proving the mechanism of O_2 reduction into H_2O_2 and the competitive relationship between H_2O reduction and O_2 reduction. What's more, the influence of catalyst concentration on photocatalytic performances were investigated. Certain mass of DAnTMS (5.0, 10.0, 15.0, 20.0, 30.0 and 40.0 mg) was dissolved in 20.0 mL MeCN with 300.0 μL added and all the reactants were irradiated for 12 h. The results are listed in Fig. 5**c & d**. When the mass of DAnTMS change from 5.0 to 15.0 mg, both the productions of H_2 and H_2O_2 exhibit the linear relationship with the catalyst mass. However, when the mass of DAnTMS reaches 20.0 mg, such linear relationship is no longer valid. This phenomenon can be ascribed to H_2O_2 poisoning effect. When the mass of DAnTMS reaches 30.0 mg or more, both the productions of H_2 and H_2O_2 reach their saturation. In order to further explore the causes, the experiment to measure the solubility of DAnTMS in MeCN was carried out. At room temperature of 25.0 ℃, the solubility of DAnTMS in MeCN was calculated to be 1.48 mg/mL. This suggests that, after the mass of DAnTMS is more than 29.6 mg, the solubility becomes an important factor that limits the activity of the photocatalyst.

3.3. *Exploration of the mechanism of the photocatalyst*

Other experiments were carried out to further explore the mechanisms of DAnTMS-mediated photocatalysis. The mechanism of H_2O_2 production was first investigated. DMPO spin-trapping electron

paramagnetic resonance (EPR) measurements were used to detect the superoxide ($\cdot O_2^-$) and hydroxyl radical ($\cdot$OH) during the photocatalytic process, displayed in Fig. 6**a & b**. The spectra suggest that$\cdot O_2^-$ and$\cdot$OH species existed in the process of photocatalysis, which indicated that photocatalytic H_2O_2 was generated through two-channel reactions [41]. Therefore, the process of DAnTMS-mediated photocatalytic oxidation of H_2O and reduction of O_2 could be confirmed.

The linear sweep voltammetry (LSV) was used to prove the capability of H^+ and O_2 reduction of DAnTMS. The LSV curves of hydrogen evolution reaction (HER) and oxygen reduction reaction (ORR) are shown in Fig. 6**c & d**, respectively. For both HER and ORR, DAnTMS shows peak at onset potential and gradually reach diffusion-limited current density, verifying the photocatalyst's HER and ORR activity.

Finally, the photocatalytic experiments of DAnTMS in commercially available MeCN ($H_2O \leq 0.01\%$) were performed to test its water removal ability. 10.0 mg DAnTMS was dissolved in 20.0 mL MeCN and irradiated for the period of time (4, 8 and 12 h). As depicted in Fig. 7**a & b**, after 12 h irradiation, 15.4 μmol H_2 and 176.7 μmol H_2O_2 are generated, the total amount of substance of which was 192.1 μmol. Considering all the possible errors, the impurity water in the MeCN solvent was completely removed according to the maximum water content (87.3 μmol). This result suggests the potential of DAnTMS to be used as a water removing agent in the organic solvents. Based on all the experiments and analysis, a reasonable schematic diagram of DAnTMS mediated photocatalysis of water splitting in MeCN is depicted in Fig. 7**c**. Under the irradiation of visible light, DAnTMS can adsorb the light and produce photogenerated carriers. Then, O_2 is reduced into H_2O_2 and H_2O is reduced into H_2 by the electrons generated on the conduction band (CB) both through the $2e^-$ pathway. Because both two reduction reactions consume electrons, a competitive relationship exists between them. However, the TPV results prove that the rate of O_2 reduction reaction is much faster than that of H_2O reduction reaction. On the other hand, H_2O is oxidated into H_2O_2 by the photogenerated holes on the valence band (VB) through the $2e^-$ pathway, and according to the TPV results, the rate of H_2O reduction is faster than that of H_2O oxidation.

4. Conclusion

In summary, an organic semiconductor of DAnTMS was used as catalyst to convert the water impurity in organic solvent into H_2 and H_2O_2 by photocatalysis. Especially, when 300.0 μL pure water was added into 20.0 mL MeCN, DAnTMS could produce H_2 with a maximum rate of 245.9 μmol g^{-1} h^{-1} and H_2O_2 with a maximum rate of 3923.4 μmol g^{-1} h^{-1}. Furthermore, a practical photocatalytic experiment with 10.0 mg DAnTMS as catalyst was also performed in 20.0 mL commercially available MeCN (98%, $H_2O \leq 0.01\%$), in which the total 15.4 μmol H_2 and 176.7 μmol H_2O_2 were produced, indicating that all the water impurity was removed. This work demonstrated the homogeneous water photo-splitting to produce clean chemical energy by organic molecular catalysts. It also provided a new promising way to remove the water impurity from organic solvents.

Associated content

Supporting Information.

Supplementary Text S1-S6; (2) Supplementary Fig. S1-S9; (3) Supplementary Tables S1.

CRediT authorship contribution statement

Zhenyu Wu: Data curation, Visualization. **Xiting Wang**: Formal analysis. **Yi Li**: Investigation, Software. **Han Zhao**: Investigation. **Jiawei Wang**: Investigation. **Hui Huang**: Project administration, Writing – original draft, Writing – review & editing, Supervision. **Yang Liu**: Resources, Writing – review & editing, Supervision. **Zhenhui Kang**: Conceptualization, Funding acquisition, Writing – review & editing, Supervision.

Declaration of Competing Interest

The authors reported no declarations of interest.

Acknowledgements

This work is supported by National MCF Energy R&D Program of China (2018YFE0306105), National Key R&D Program of China (2020YFA0406104, 2020YFA0406101), Innovative Research Group Project of the National Natural Science Foundation of China (51821002), National Natural Science Foundation of China (51725204, 21771132, 51972216, 52041202), Natural Science Foundation of Jiangsu Province (BK20190041), Key-Area Research and Development Program of GuangDong Province (2019B010933001), Collaborative Innovation Center of Suzhou Nano Science & Technology, the 111 Project, and Suzhou Key Laboratory of Functional Nano & Soft Materials.

Appendix A. Supporting information

Supplementary data associated with this article can be found in the online version at doi:10.1016/j.apcatb.2021.121047.

References

[1] M. Gryszel, R. Rybakiewicz, E.D. Głowacki, Water-soluble organic dyes as molecular photocatalysts for H_2O_2 evolution, Adv. Sustain. Syst. 3 (2019), https://doi.org/10.1002/adsu.201900027.

[2] F. Guo, W. Shi, C. Zhu, H. Li, Z. Kang, CoO and g-C_3N_4 complement each other for highly efficient overall water splitting under visible light, Appl. Catal. B Environ. 226 (2018) 412–420, https://doi.org/10.1016/j.apcatb.2017.12.064.

[3] H. Lan, Y. Xia, K. Feng, A. Wei, Z. Kang, J. Zhong, Co-doped carbon layer to lower the onset potential of hematite for solar water oxidation, Appl. Catal. B Environ. 258 (2019), https://doi.org/10.1016/j.apcatb.2019.117962.

[4] M. Zbiri, C.M. Aitchison, R.S. Sprick, A.I. Cooper, A.A.Y. Guilbert, Probing dynamics of water mass transfer in organic porous photocatalyst water-splitting materials by neutron spectroscopy, Chem. Mater. 33 (2021) 1363–1372, https://doi.org/10.1021/acs.chemmater.0c04425.

[5] X. Zhu, Z. Song, Z. Wang, W. Liu, B. Hong, J. Bao, C. Gao, S. Sun, Selective formation of interfacial bonding enables superior hydrogen production in organic–inorganic hybrid cocatalyzed photocatalysts, Appl. Catal. B Environ. 274 (2020), https://doi.org/10.1016/j.apcatb.2020.119010.

[6] Y. Liu, Y. Zhao, Q. Wu, X. Wang, H. Nie, Y. Zhou, H. Huang, M. Shao, Y. Liu, Z. Kang, Charge storage of carbon dot enhances photo-production of H_2 and H_2O_2 over Ni_2P/carbon dot catalyst under normal pressure, Chem. Eng. J. 409 (2021), https://doi.org/10.1016/j.cej.2020.128184.

[7] L. Wang, G. Zhou, Y. Tian, L. Yan, M. Deng, B. Yang, Z. Kang, H. Sun, Hydroxyl decorated g-C_3N_4 nanoparticles with narrowed bandgap for high efficient photocatalyst design, Appl. Catal. B Environ. 244 (2019) 262–271, https://doi.org/10.1016/j.apcatb.2018.11.054.

[8] Y. Liu, Y. Zhao, Y. Sun, J. Cao, H. Wang, X. Wang, H. Huang, M. Shao, Y. Liu, Z. Kang, A 4e-–2e- cascaded pathway for highly efficient production of H_2 and H_2O_2 from water photo-splitting at normal pressure, Appl. Catal. B Environ. 270 (2020), https://doi.org/10.1016/j.apcatb.2020.118875.

[9] Y. Peng, L. Wang, Y. Liu, H. Chen, J. Lei, J. Zhang, Visible-light-driven photocatalytic H_2O_2 production on g-C_3N_4 loaded with CoP as a noble metal free cocatalyst, Eur. J. Inorg. Chem. 2017 (2017) 4797–4802, https://doi.org/10.1002/ejic.201700930.

[10] Y. Li, C. Gao, W. Jiang, C. Zhuang, W. Tan, W. Li, Y. Li, L. Wang, X. Liao, Z. Sun, J. Zou, X. Han, A game-changing design of low-cost, large-size porous cocatalysts decorated by ultra-small photocatalysts for highly efficient hydrogen evolution, Appl. Catal. B Environ. 286 (2021), https://doi.org/10.1016/j.apcatb.2021.119923.

[11] V. Datsyuk, M. Kalyva, K. Papagelis, J. Parthenios, D. Tasis, A. Siokou, I. Kallitsis, C. Galiotis, Chemical oxidation of multiwalled carbon nanotubes, Carbon 46 (2008) 833–840, https://doi.org/10.1016/j.carbon.2008.02.012.

[12] S. Yanagida, A. Kabumoto, K. Mizumoto, C. Pac, Poly(p-phenylene)-catalysed photoreduction of water to hydrogen, J. Chem. Soc. Chem. Commun. (1985) 474–475, https://doi.org/10.1039/c39850000474.

[13] J. Kosco, F. Moruzzi, B. Willner, I. McCulloch, Photocatalysts based on organic semiconductors with tunable energy levels for solar fuel applications, Adv. Energy Mater. 10 (2020), https://doi.org/10.1002/aenm.202001935.

[14] J. Liang, X. Yang, Y. Wang, P. He, H. Fu, Y. Zhao, Q. Zou, X. An, A review on g-C_3N_4 incorporated with organics for enhanced photocatalytic water splitting, J. Mater. Chem. A 9 (2021) 12898–12922, https://doi.org/10.1039/d1ta00890k.
[15] R.S. Sprick, Z. Chen, A.J. Cowan, Y. Bai, C.M. Aitchison, Y. Fang, M. A. Zwijnenburg, A.I. Cooper, X. Wang, Water oxidation with cobalt-loaded linear conjugated polymer photocatalysts, Angew. Chem. Int. Ed. 59 (2020) 18695–18700, https://doi.org/10.1002/anie.202008000.
[16] Z. Wei, M. Liu, Z. Zhang, W. Yao, H. Tan, Y. Zhu, Efficient visible-light-driven selective oxygen reduction to hydrogen peroxide by oxygen-enriched graphitic carbon nitride polymers, Energy Environ. Sci. 11 (2018) 2581–2589, https://doi.org/10.1039/c8ee01316k.
[17] C. Shu, Y. Zhao, C. Zhang, X. Gao, W. Ma, S.B. Ren, F. Wang, Y. Chen, J.H. Zeng, J. X. Jiang, Bisulfone-functionalized organic polymer photocatalysts for high-performance hydrogen evolution, ChemSusChem 13 (2020) 369–375, https://doi.org/10.1002/cssc.201902797.
[18] L. Gubicza, N. Nemestóthy, T. Fráter, K. Bélafi-Bakó, Enzymatic esterification in ionic liquids integrated with pervaporation for water removal, Green Chem. 5 (2003), https://doi.org/10.1039/b211342m.
[19] B. Burrichter, C. Pasel, M. Luckas, D. Bathen, Parameter study on the adsorptive drying of isopropanol in a fixed bed adsorber, Sep. Purif. Technol. 132 (2014) 736–743, https://doi.org/10.1016/j.seppur.2014.06.030.
[20] T. Lanjewar, P. Badwaik, M.N. Varma, Removal of water from the spent mixture of nitric-sulfuric acid by using silicon carbide ceramic diffusive membrane, Sep. Purif. Technol. 265 (2021), https://doi.org/10.1016/j.seppur.2021.118426.
[21] Q. Zhang, P. Shi, A. Zeng, Y. Ma, X. Yuan, Dynamic control analysis of intensified extractive distillation process with vapor recompression, Sep. Purif. Technol. 233 (2020), https://doi.org/10.1016/j.seppur.2019.116016.
[22] M. Gavahian, P.E.S. Munekata, I. Eş, J.M. Lorenzo, A. Mousavi Khaneghah, F. J. Barba, Emerging techniques in bioethanol production: from distillation to waste valorization, Green Chem. 21 (2019) 1171–1185, https://doi.org/10.1039/c8gc02698j.
[23] B. Yan, L. Zhang, Z. Tang, M. Al-Mamun, H. Zhao, X. Su, Palladium-decorated hierarchical titania constructed from the metal-organic frameworks NH_2-MIL-125 (Ti) as a robust photocatalyst for hydrogen evolution, Appl. Catal. B Environ. 218 (2017) 743–750, https://doi.org/10.1016/j.apcatb.2017.07.020.
[24] X. Gu, Z. Chen, Y. Li, J. Wu, X. Wang, H. Huang, Y. Liu, B. Dong, M. Shao, Z. Kang, Polyaniline/carbon dots composite as a highly efficient metal-free dual-functional photoassisted electrocatalyst for overall water splitting, ACS Appl. Mater. Interfaces 13 (2021) 24814–24823, https://doi.org/10.1021/acsami.1c04386.
[25] X. Wang, W. Bian, Y. Ma, Y. Liu, Z. Wang, C. Shi, H. Lin, Y. Liu, H. Huang, Z. Kang, Hydroxyl-terminated carbon dots for efficient conversion of cyclohexane to adipic acid, J. Colloid Interface Sci. 591 (2021) 281–289, https://doi.org/10.1016/j.jcis.2021.02.021.
[26] N. Baig, S. Shetty, S. Al-Mousawi, B. Alameddine, Synthesis of conjugated polymers via cyclopentannulation reaction: promising materials for iodine adsorption, Polym. Chem. 11 (2020) 3066–3074, https://doi.org/10.1039/d0py00286k.
[27] C. Zhu, Ca Liu, Y. Fu, J. Gao, H. Huang, Y. Liu, Z. Kang, Construction of CDs/CdS photocatalysts for stable and efficient hydrogen production in water and seawater, Appl. Catal. B Environ. 242 (2019) 178–185, https://doi.org/10.1016/j.apcatb.2018.09.096.
[28] S. Ratso, I. Kruusenberg, A. Sarapuu, P. Rauwel, R. Saar, U. Joost, J. Aruväli, P. Kanninen, T. Kallio, K. Tammeveski, Enhanced oxygen reduction reaction activity of iron-containing nitrogen-doped carbon nanotubes for alkaline direct methanol fuel cell application, J. Power Sources 332 (2016) 129–138, https://doi.org/10.1016/j.jpowsour.2016.09.069.
[29] J.L.C. Fonseca, S. Tasker, D.C. Apperley, J.P.S. Badyal, Plasma-enhanced chemical vapor deposition of organosilicon materials: a comparison of hexamethyldisilane and tetramethylsilane precursors, Macromolecules 29 (1996) 1705–1710, https://doi.org/10.1021/ma950222v.
[30] K.L. Smith, K.M. Black, Characterization of the treated surfaces of silicon alloyed pyrolytic carbon and SiC, J. Vac. Sci. Technol. A Vac. Surf. Films 2 (1984) 744–747, https://doi.org/10.1116/1.572562.
[31] M.Z. Rahman, M.G. Kibria, C.B. Mullins, Metal-free photocatalysts for hydrogen evolution, Chem. Soc. Rev. 49 (2020) 1887–1931, https://doi.org/10.1039/c9cs00313d.
[32] Y. Kofuji, S. Ohkita, Y. Shiraishi, H. Sakamoto, S. Tanaka, S. Ichikawa, T. Hirai, Graphitic carbon nitride doped with biphenyl diimide: efficient photocatalyst for hydrogen peroxide production from water and molecular oxygen by sunlight, ACS Catal. 6 (2016) 7021–7029, https://doi.org/10.1021/acscatal.6b02367.
[33] Y. Zheng, H. Wei, P. Liang, X. Xu, X. Zhang, H. Li, C. Zhang, C. Hu, X. Zhang, B. Lei, W.Y. Wong, Y. Liu, J. Zhuang, Near-infrared-excited multicolor afterglow in carbon dots-based room-temperature afterglow materials, Angew. Chem. Int. Ed. 60 (2021) 22253–22259, https://doi.org/10.1002/anie.202108696.
[34] J.S.A. Ishibashi, C. Darrigan, A. Chrostowska, B. Li, S.Y. Liu, A BN anthracene mimics the electronic structure of more highly conjugated systems, Dalton Trans. 48 (2019) 2807–2812, https://doi.org/10.1039/c9dt00481e.
[35] J. Cao, Q. Wu, Y. Zhao, K. Wei, Y. Li, X. Wang, F. Liao, H. Huang, M. Shao, Y. Liu, Z. Kang, In-situ photovoltage transients assisted catalytic study on H_2O_2 photoproduction over organic molecules modified carbon nitride photocatalyst, Appl. Catal. B Environ. 285 (2021), https://doi.org/10.1016/j.apcatb.2020.119817.
[36] Y. Li, Y. Zhao, H. Nie, K. Wei, J. Cao, H. Huang, M. Shao, Y. Liu, Z. Kang, Interface photo-charge kinetics regulation by carbon dots for efficient hydrogen peroxide production, J. Mater. Chem. A 9 (2021) 515–522, https://doi.org/10.1039/d0ta10231h.
[37] Q. Wu, Y. Liu, J. Cao, Y. Sun, F. Liao, Y. Liu, H. Huang, M. Shao, Z. Kang, A function-switchable metal-free photocatalyst for the efficient and selective production of hydrogen and hydrogen peroxide, J. Mater. Chem. A 8 (2020) 11773–11780, https://doi.org/10.1039/d0ta03974h.
[38] Q. Liang, L. Liu, Z. Wu, H. Nie, H. Shi, Z. Li, Z. Kang, Polytriptycene@CdS double shell hollow spheres with enhanced interfacial charge transfer for highly efficient photocatalytic hydrogen evolution, J. Mater. Chem. A 9 (2021) 9105–9112, https://doi.org/10.1039/d1ta01081f.
[39] Q. Liang, S. Zhao, Z. Li, Z. Wu, H. Shi, H. Huang, Z. Kang, Converting organic wastewater into CO using MOFs-derived Co/In_2O_3 double-shell photocatalyst, ACS Appl. Mater. Interfaces 13 (2021) 40754–40765, https://doi.org/10.1021/acsami.1c12800.
[40] H. Nie, K. Wei, Y. Li, Y. Liu, Y. Zhao, H. Huang, M. Shao, Y. Liu, Z. Kang, Carbon dots/Bi_2WO_6 composite with compensatory photo-electronic effect for overall water photo-splitting at normal pressure, Chin. Chem. Lett. (2021), https://doi.org/10.1016/j.cclet.2021.01.041.
[41] Y. Zhao, Y. Liu, J. Cao, H. Wang, M. Shao, H. Huang, Y. Liu, Z. Kang, Efficient production of H_2O_2 via two-channel pathway over ZIF-8/C_3N_4 composite photocatalyst without any sacrificial agent, Appl. Catal. B Environ. 278 (2020), https://doi.org/10.1016/j.apcatb.2020.119289.